Electronic Supplementary Material (ESI) for Journal of Materials Chemistry C.

Supporting information

Wearable, waterproof, and highly sensitive strain sensor based on three-dimensional graphene/carbon black/Ni sponge for wirelessly monitoring human motions

Shibin Sun[1], Yiqian Liu[1], Xueting Chang[2*], Yingchang Jiang[2], Dongsheng Wang[2], Chengji Tang[1], Shiyu He[1], Mingwei Wang[1], Lin Guo[1], Yang Gao[3*]

[1] *School of Logistics Engineering, Shanghai Maritime University, Shanghai 201306, China*

[2] *Institute of Marine Materials Science and Engineering, School of Ocean Science and Engineering, Shanghai Maritime University, Shanghai 201306, China*

[3]*School of Mechanical and Power Engineering, East China University of Science and Technology, Shanghai 200237, China*

[*] Corresponding author. E-mail: xtchang@shmtu.edu.cn, yanggao@ecust.edu.cn.

Fig. S1 Photos of a long G/CB/Ni sensor that was folded into a butterfly knot shape.

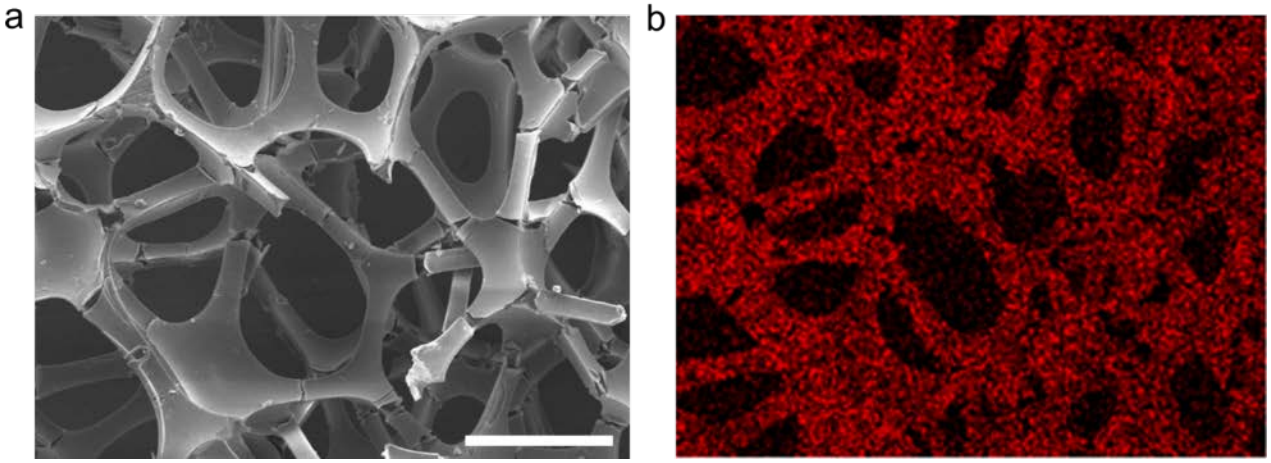

Fig. S2 (a) SEM image of pure Ni sponge and (b) Ni mapping. Scale bar in (a) is 100 μm.

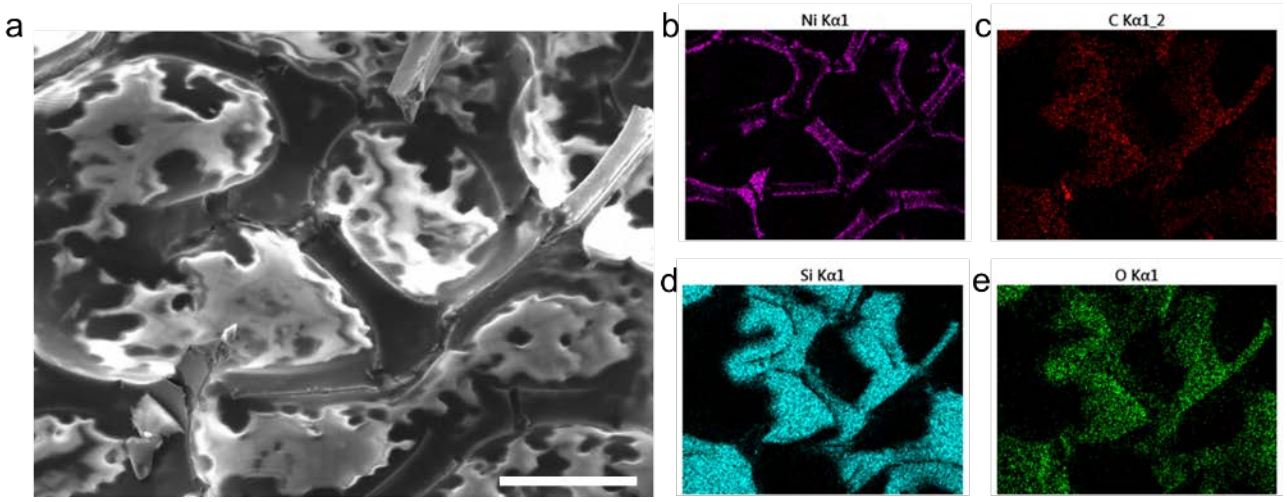

Fig. S3 (a) SEM image of CB/Ni sensor and the corresponding EDS mapping of (b) Ni, (c) C, and (d) Si, and (e) O elements. Scale bars in (a) is 200 μm, respectively.

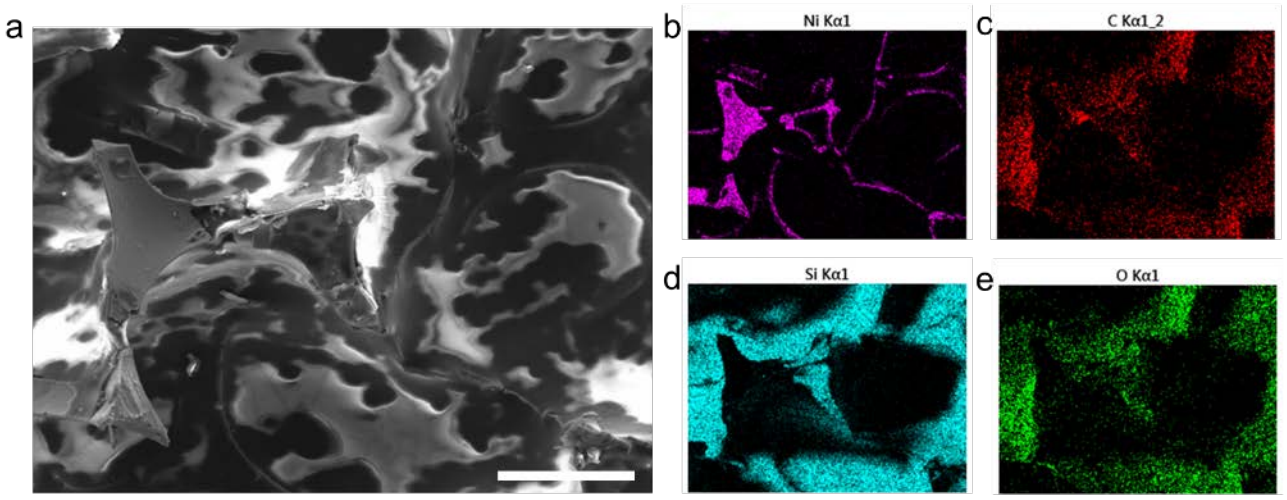

Fig. S4 (a) SEM image of G/Ni sensor and the corresponding EDS mapping of (b) Ni, (c) C, and (d) Si, and (e) O elements. Scale bars in (a) is 200 μm, respectively.

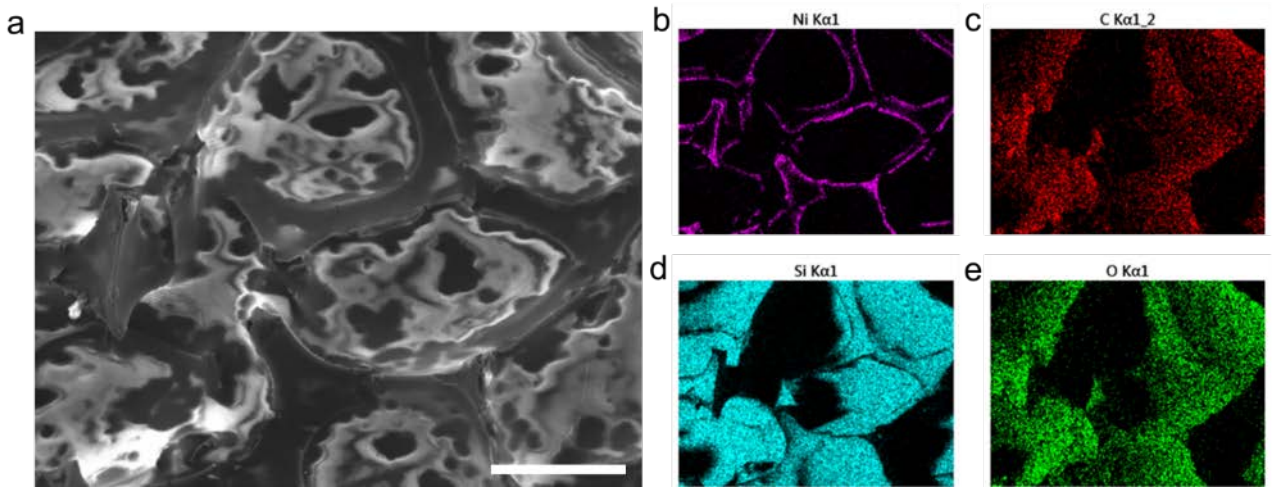

Fig. S5 (a) SEM image of G/CB/Ni-0.5 sensor and the corresponding EDS mapping of (b) Ni, (c) C, and (d) Si, and (e) O elements. Scale bar in (a) is 100 μm.

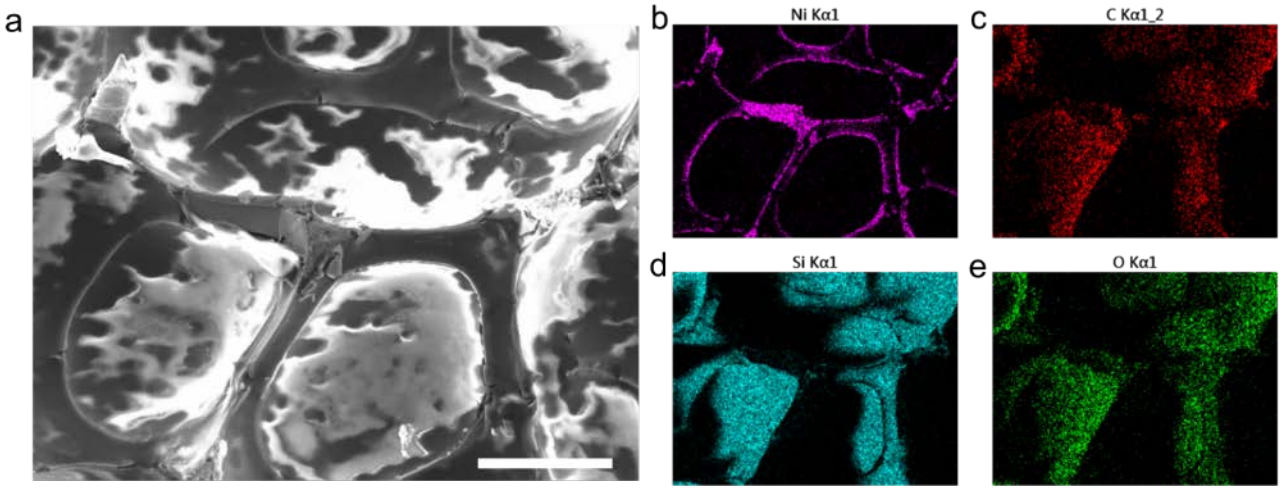

Fig. S6 (a) SEM image of G/CB/Ni-1 sensor and the corresponding EDS mapping of (b) Ni, (c) C, and (d) Si, and (e) O elements. Scale bar in (a) is 100 μm.

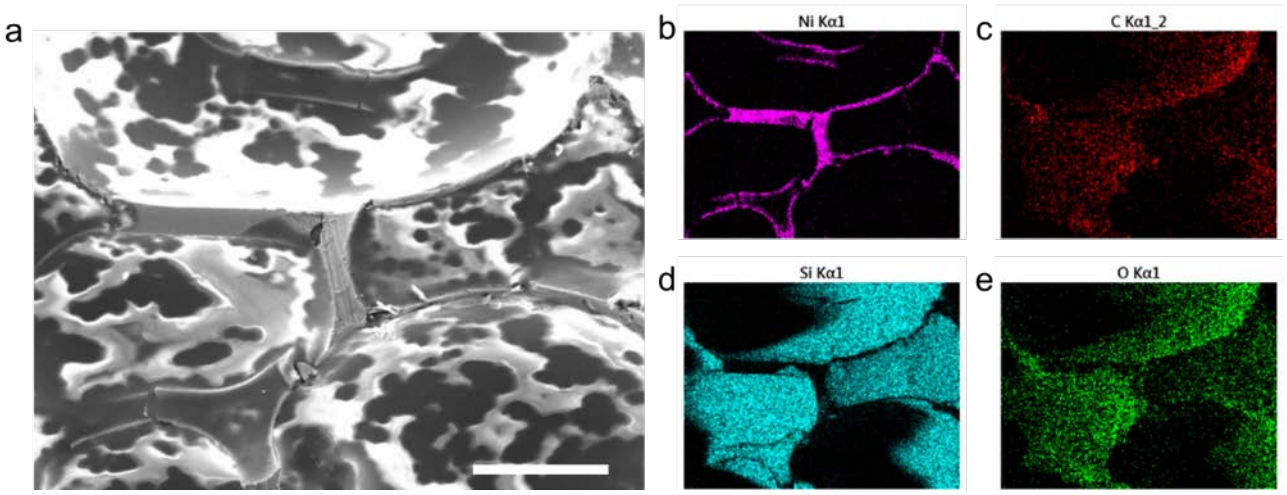

Fig. S7 (a) SEM image of G/CB/Ni-3 sensor and the corresponding EDS mapping of (b) Ni, (c) C, and (d) Si, and (e) O elements. Scale bar in (a) is 100 μm.

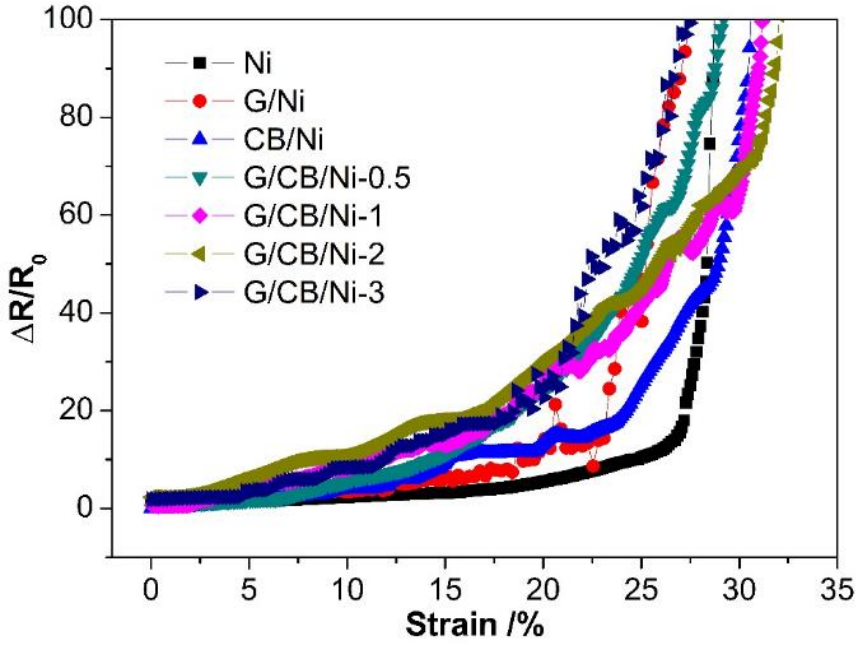

Fig. S8 Typical relative resistance change as a function of applied strains for the (a) Ni, (b) G/Ni, (c) CB/Ni, (d) G/CB/Ni-0.5, (e) G/CB/Ni-1, and (f) G/CB/Ni-3 sensors.

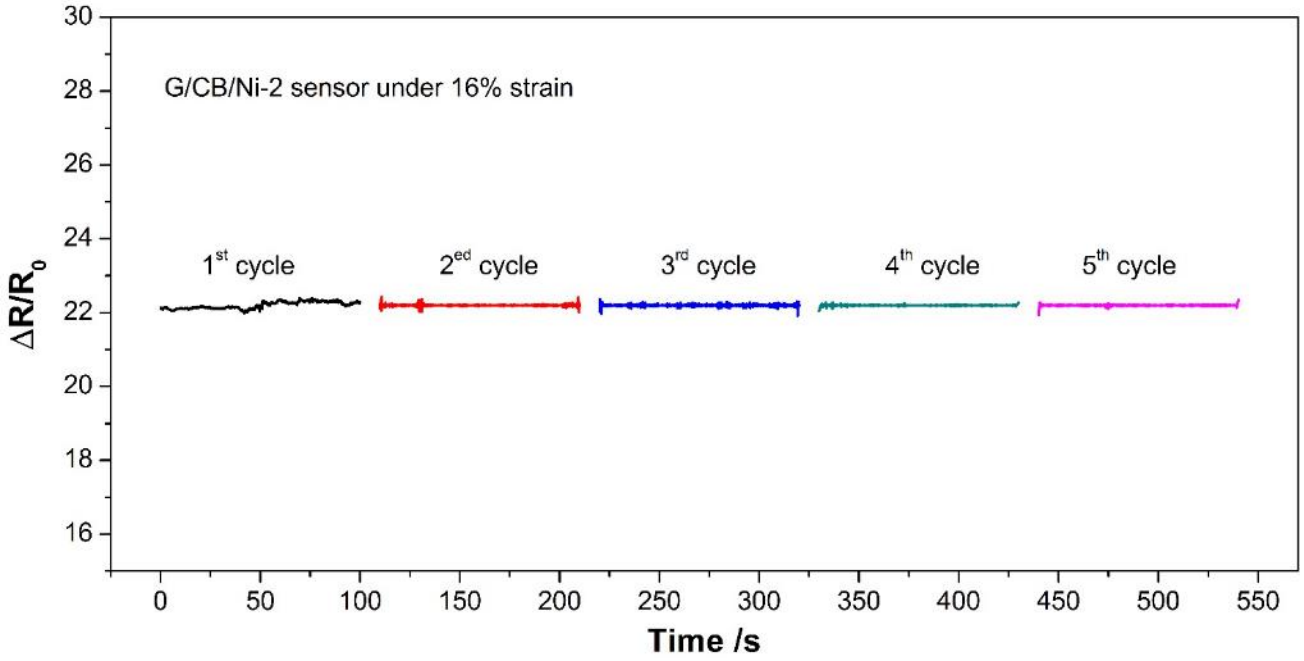

Fig. S9 Cyclic $\Delta R/R_0$ *vs* time curves of G/CB/Ni-2 sensor under 16% strain.

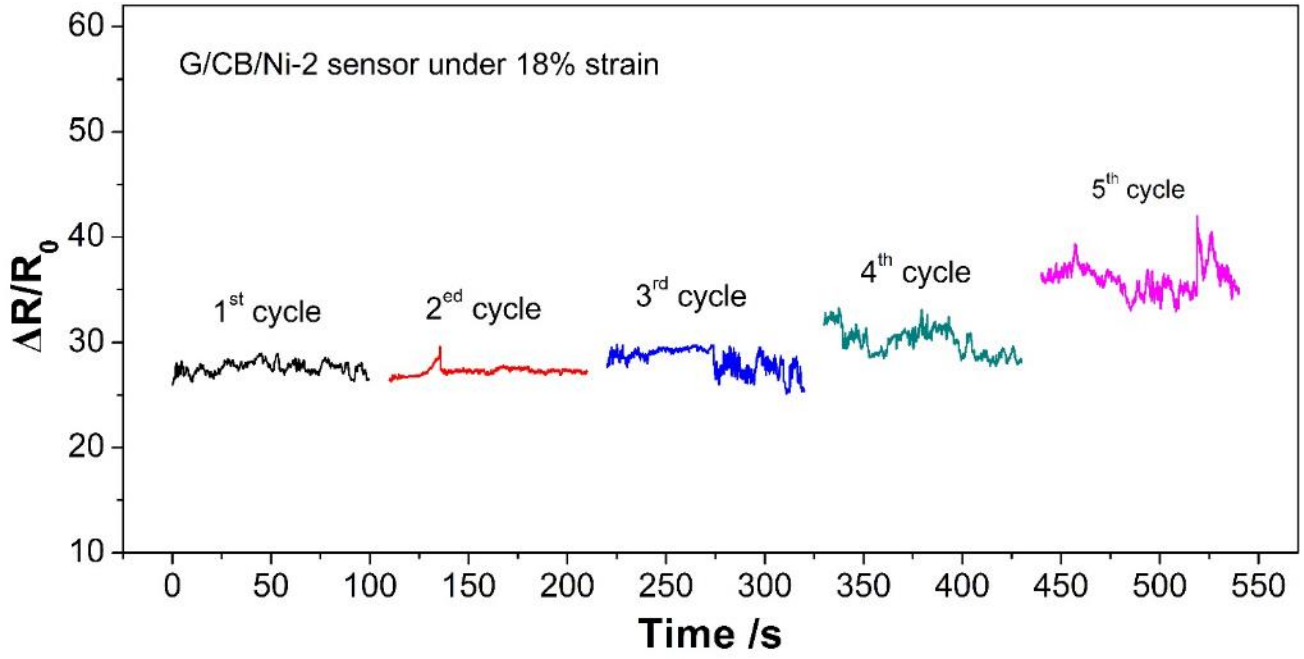

Fig. S10 Cyclic $\Delta R/R_0$ *vs* time curves of G/CB/Ni-2 sensor under 18% strain.

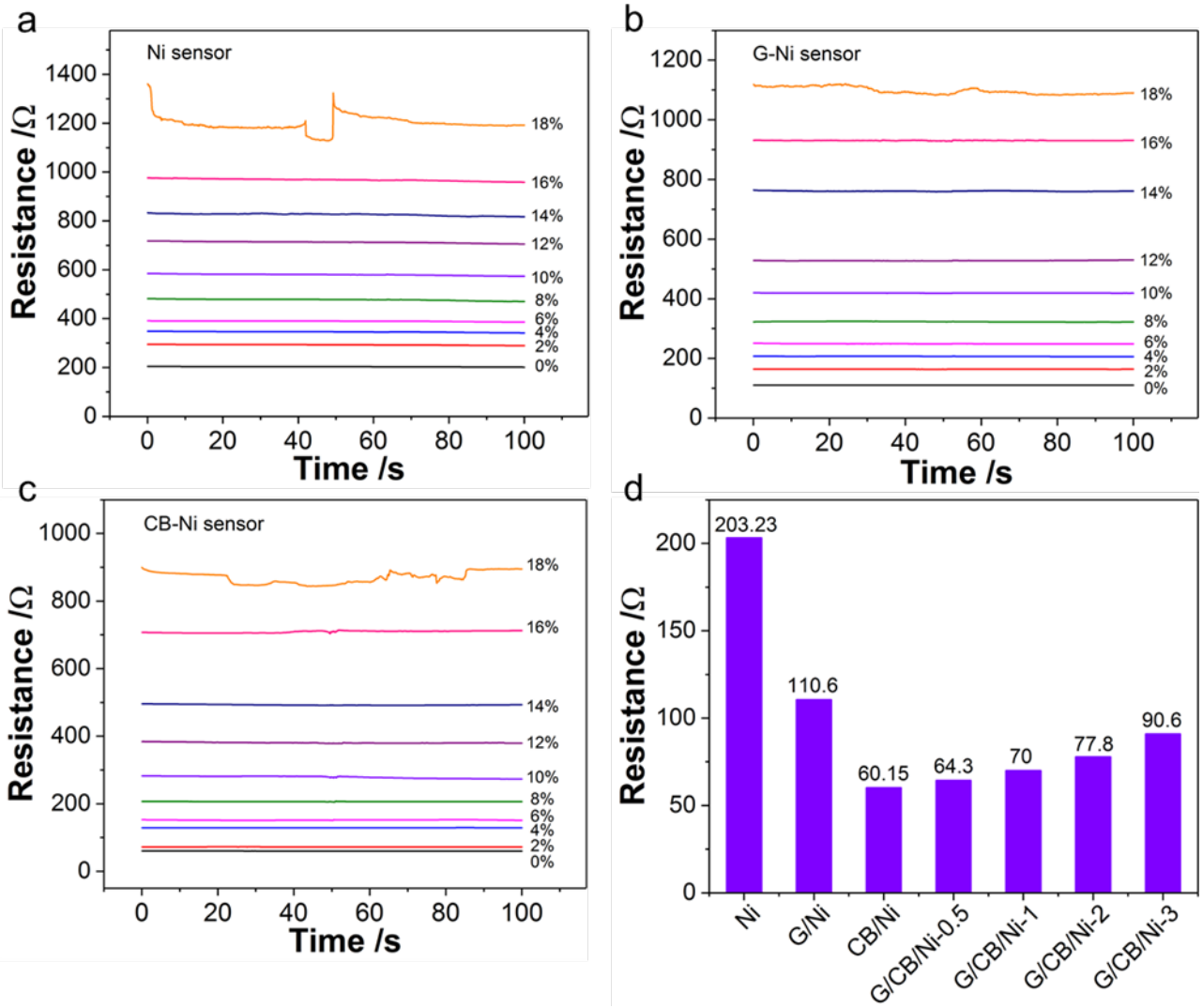

Fig. S11 Time-dependent resistance curves of (a) Ni, (b) G/Ni, and (c) CB/Ni under 0-18% strain. (d) Comparison of the original resistance of different sensors.

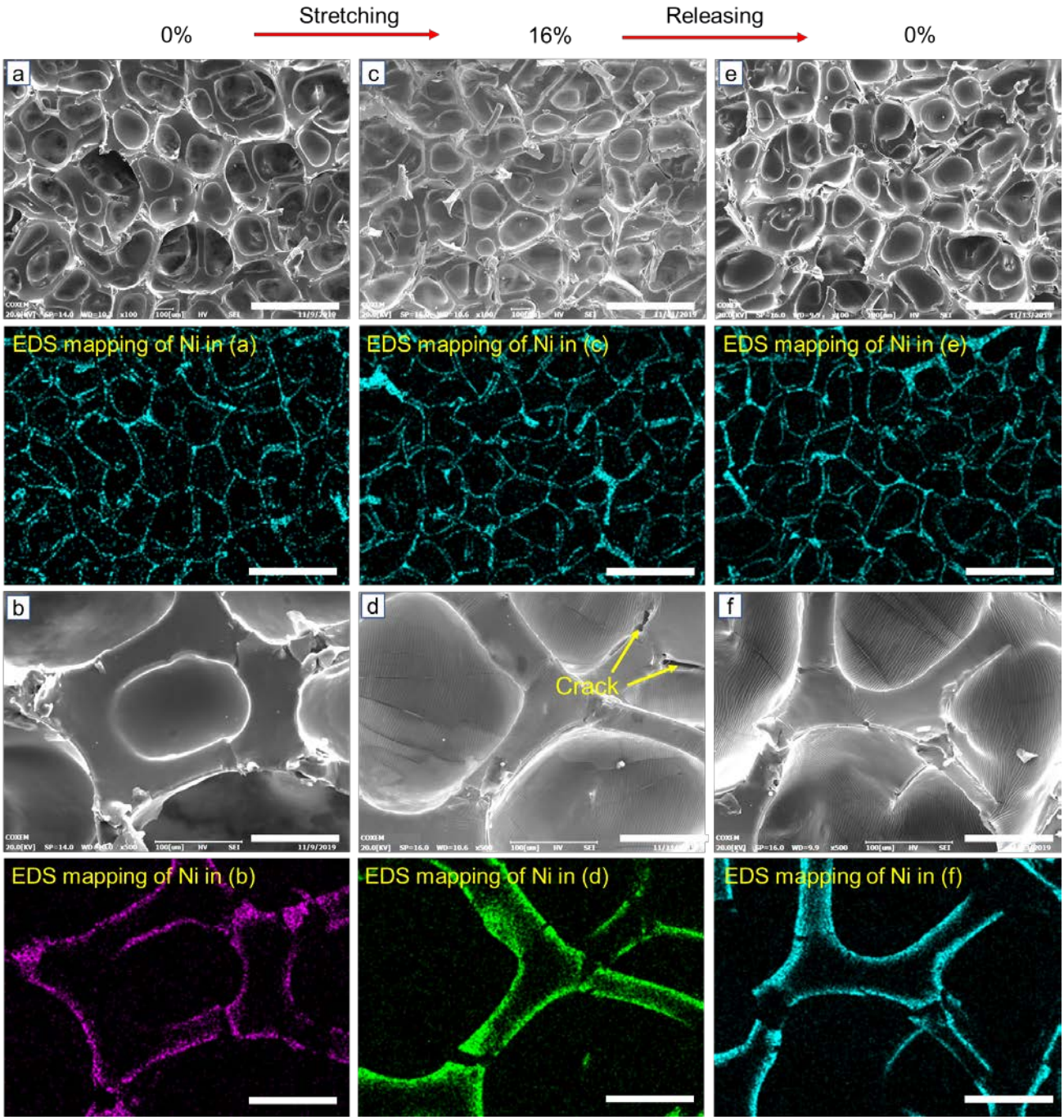

Fig. S12 Top-view SEM images and the corresponding EDS mapping of Ni element for the G/CB/Ni-2 sensor at different stages during the stretching-releasing process: (a, b) 0% strain, (c, d) 16% strain, and (e, f) released to 0% strain. Scale bars in (a), (c), and (e) are 500 μm. Scale bars in (b), (d), and (f) are 100 μm.

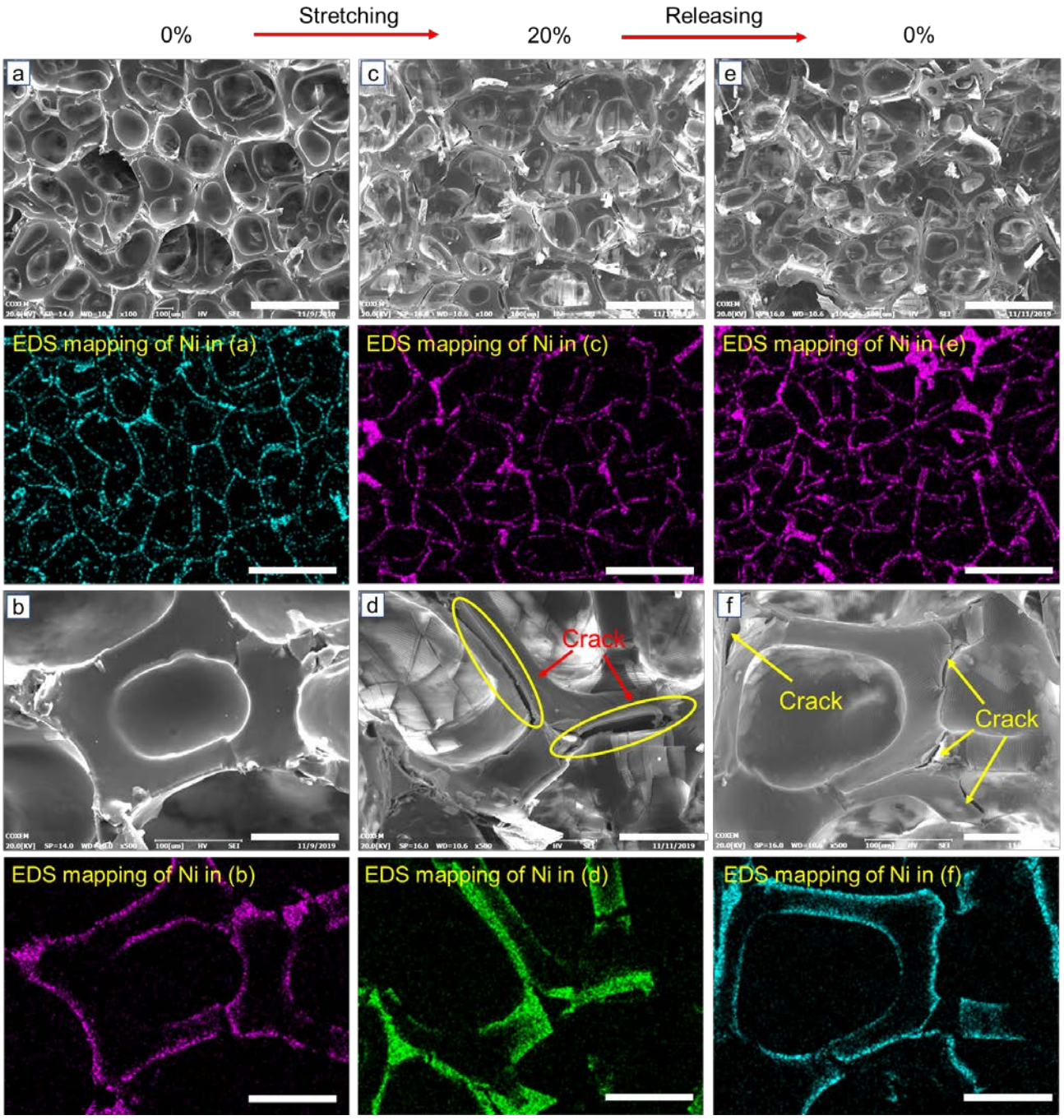

Fig. S13 Top-view SEM images and the corresponding EDS mapping of Ni element for the G/CB/Ni-2 sensor at different stages during the stretching-releasing process: (a, b) 0% strain, (c, d) 20% strain, and (e, f) released to 0% strain. Scale bars in (a), (c), and (e) are 500 μm. Scale bars in (b), (d), and (f) are 100 μm.

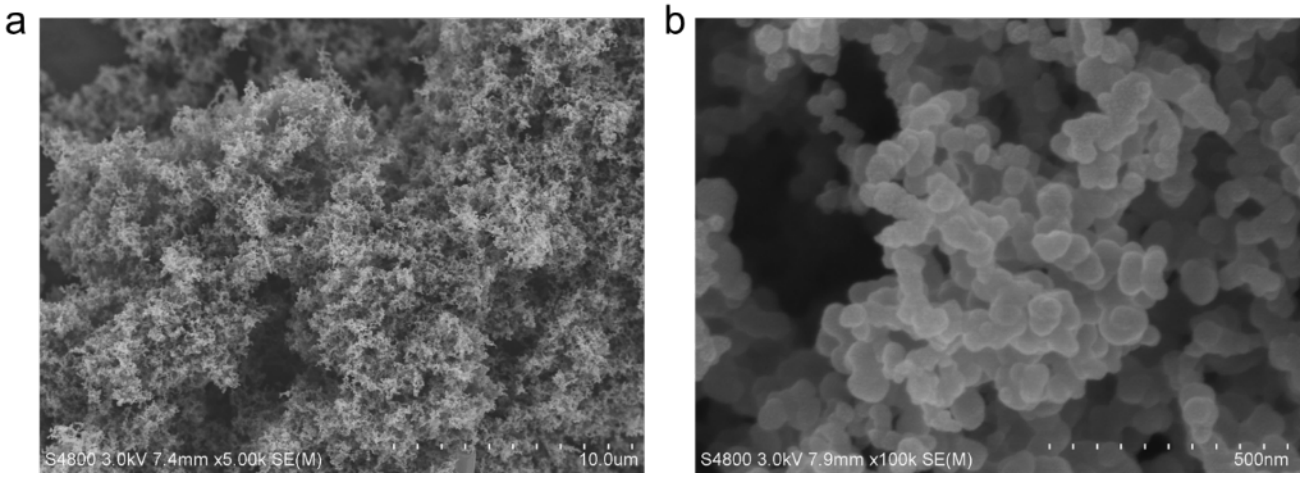

Fig. S14 SEM images of CB.

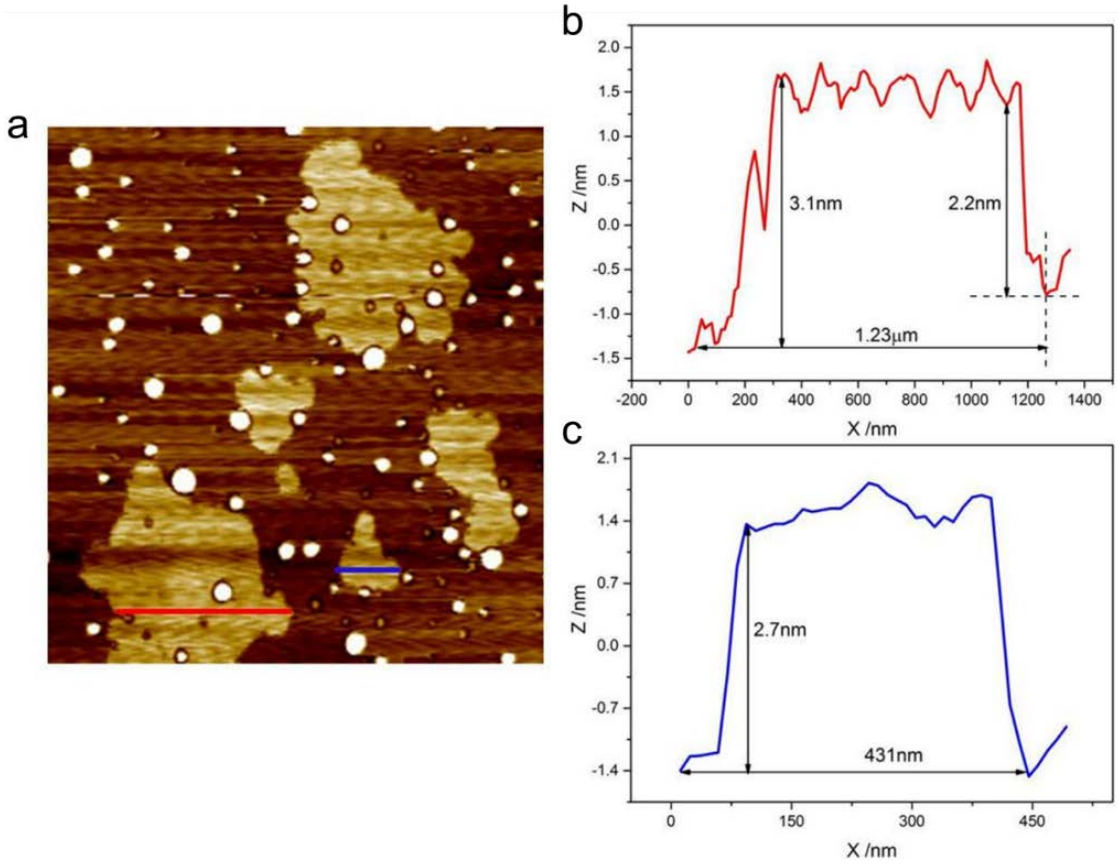

Fig. S15 (a) AFM image and (b, c) height profiles of G. The height profiles in (b) and (c) correspond to the red and blue lines in (a), respectively.

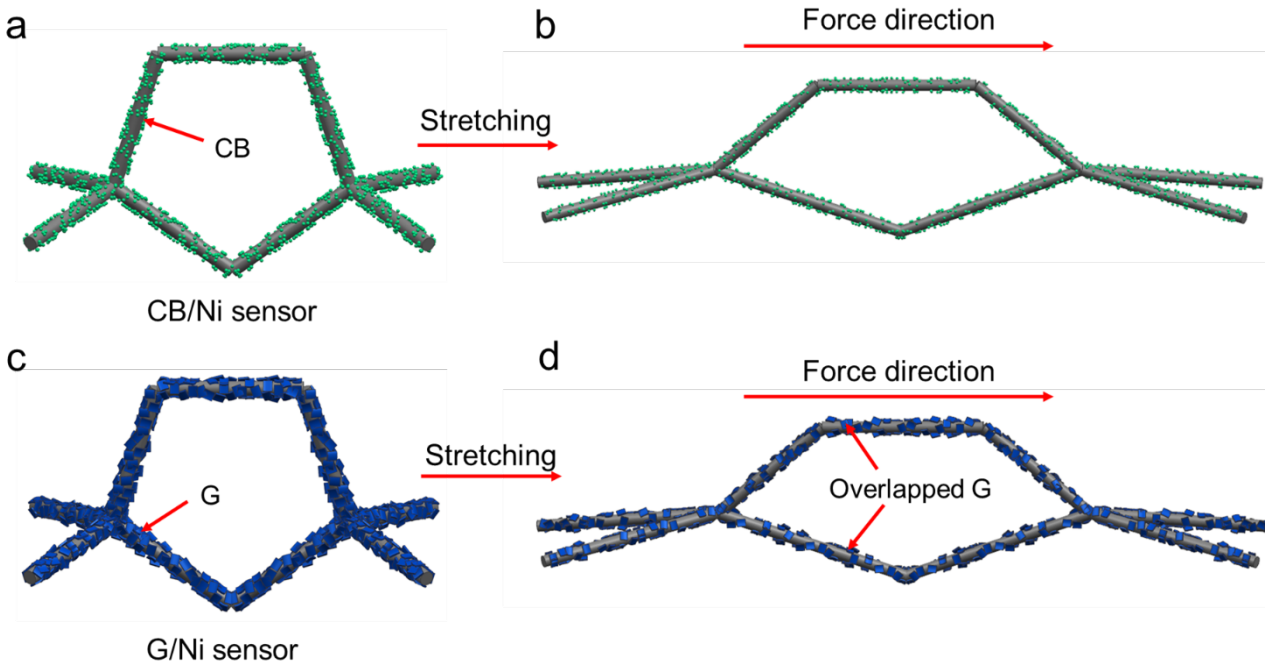

Fig. S16 Schematics of local structures of unstretched and stretched sensors: (a, b) G/Ni sensor and (c, d) CB/Ni sensor.

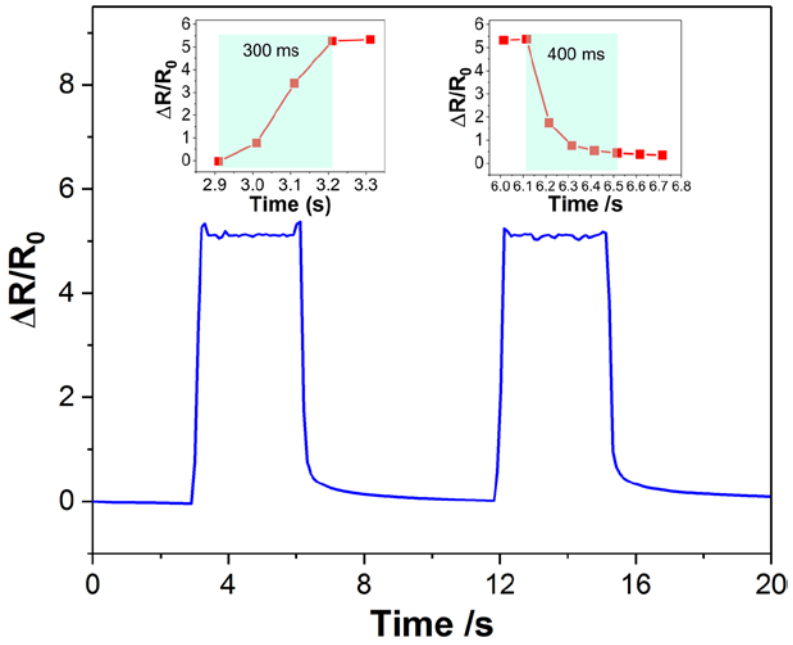

Fig. S17 Relative resistance change of G/CB/Ni-2 sensor upon cycling under a strain of 4%.

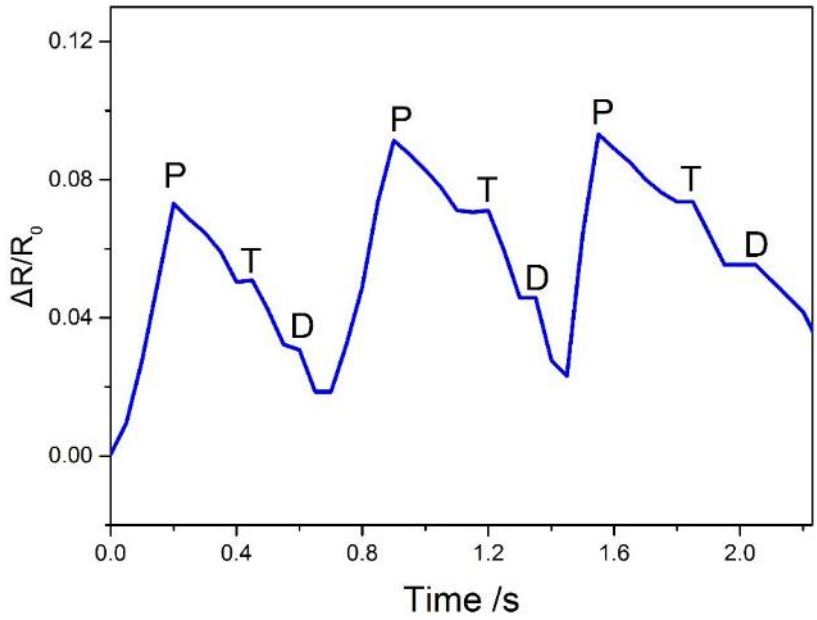

Fig. S18 Enlarged response signals of pulse. It is clear that a single pulse is composed of three peaks, which corresponds to the percussion wave (P-wave), tidal wave (T-wave), and diastolic wave (D-wave) of a pulse waveform.

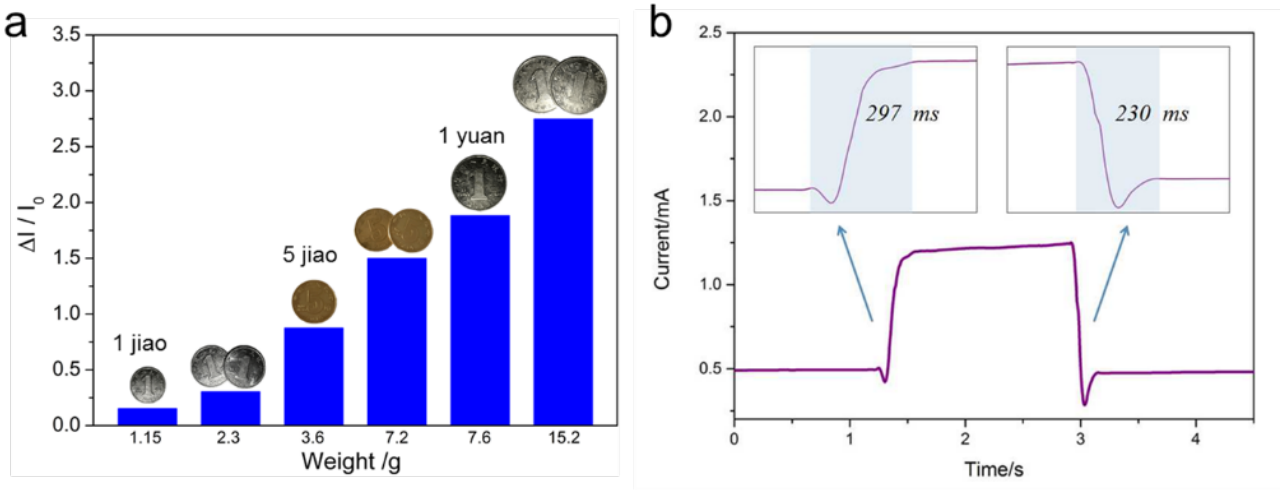

Fig. S19 Sensing performance of G/CB/Ni-2 sensor towards pressure and bending stress. (a) Relative current changes ($\Delta I/I_0$) of G/CB/Ni-2 sensor as a function of weight and (b) response and recovery times of G/CB/Ni-2 sensor towards pressure.

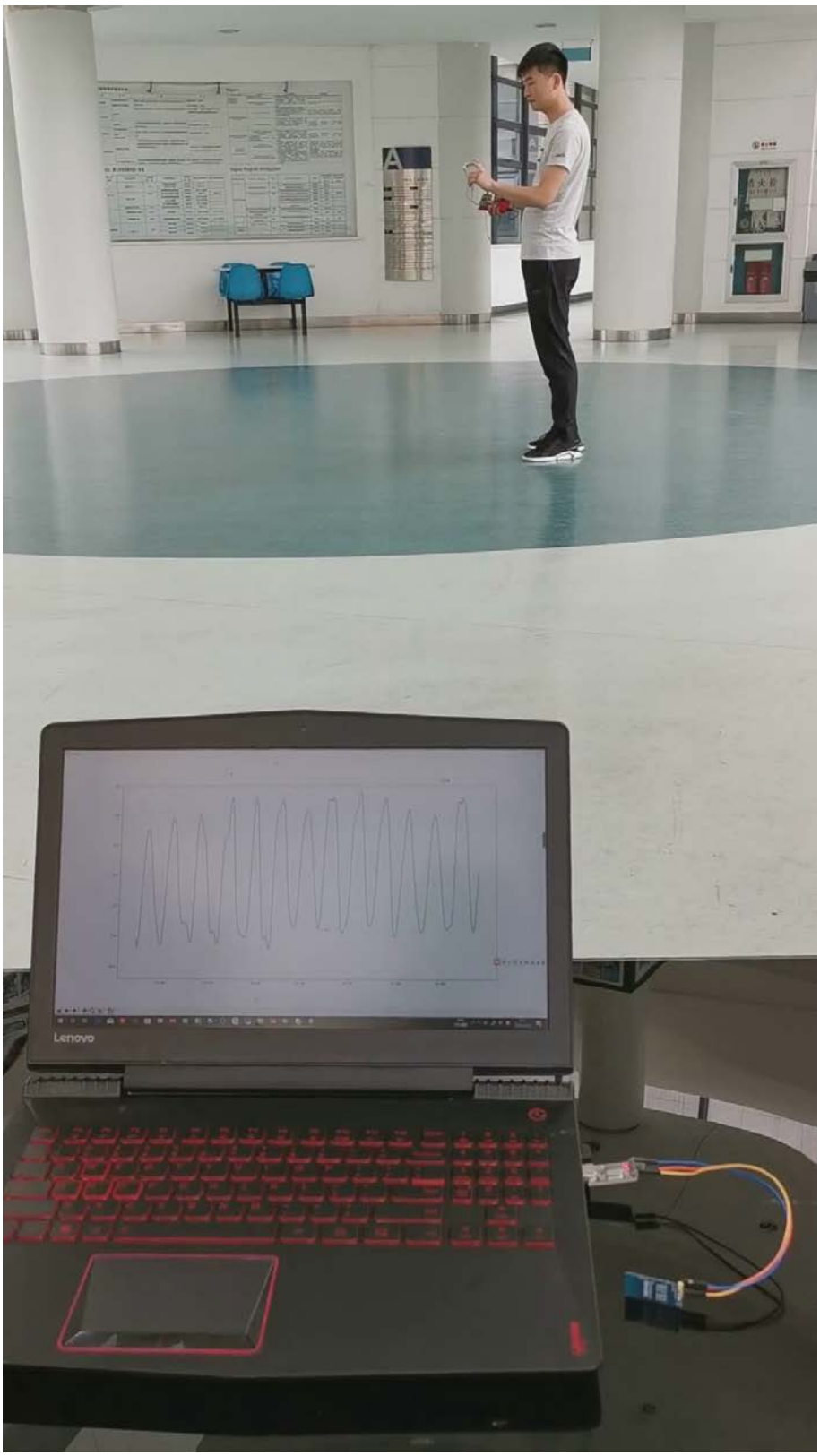

Fig. S20 Photo of the computer with electrical signals on the screen and the tester who wore the sensor on the elbow joint and held the circuit board and power source.

Fig. S21 Testing of the wireless sensor system outdoors.

The photo shows that the tester wearing the sensor was walking outdoors. At this moment, the distance between the walker and the computer connected with the ZigBee receiver was about 50 m. The electrical signals were displayed on the computer screen.

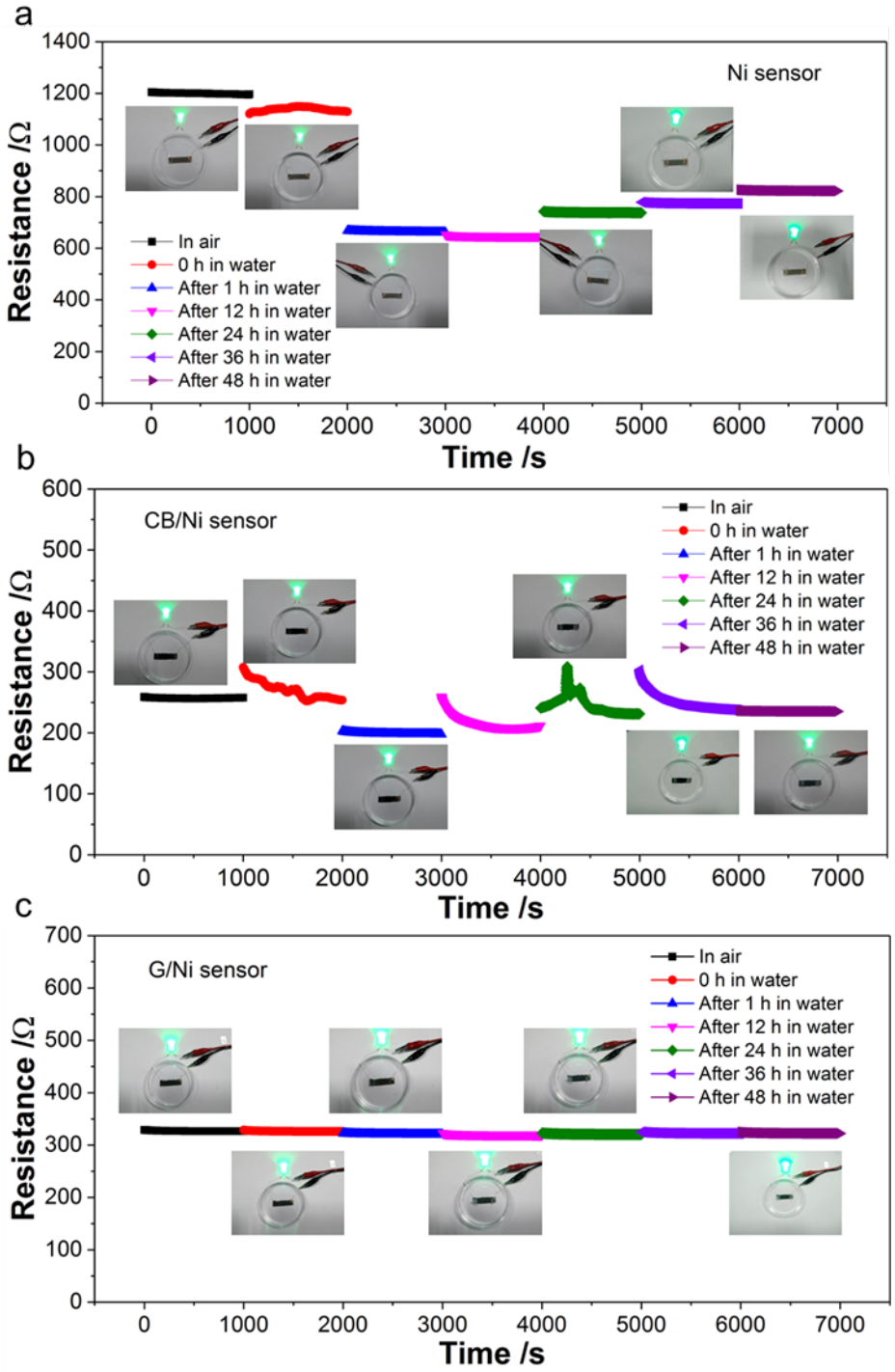

Fig. S22 Time-dependent resistance curves of (a) Ni sensor, (b) CB/Ni sensor, and (c) G/Ni sensor in air and in water (0-48 h). Insets are the photos of the sensors acting as interconnectors to light up the LED.

It can be seen that the water had obvious influence on the resistance of the Ni sensor (Fig. S21a) and CB/Ni sensor (Fig. S21b). When the two samples were just immersed in the water (0 h), noticeable resistance fluctuations happened. Then, the resistance changed obviously with increasing immersing

time (1-48 h). Though the resistance change of the Ni and CB/Ni sensors cannot influence the working of the LED, it would significantly influence the sensing accuracy for monitoring subtle motions because their initial resistances were low. Thus, both the Ni and CB/Ni sensors are unsuitable for waterproof applications. Similar to the G/CB/Ni-2 sensor, the G/Ni sensor (Fig. S21c) also demonstrated outstanding waterproof performance since its resistance remained unchanged during the test.